

Influence of chemical doping and hydrostatic pressure on the magnetic properties of $\text{Mn}_{1-x}\text{Fe}_x\text{As}$ magnetocaloric compounds

D. L. Rocco,^{1,*} A. de Campos,² A. Magnus G. Carvalho,³ A. O. dos Santos,⁴ L. M. da Silva,⁴ S. Gama,⁵ M. S. da Luz,² P. von Ranke,⁶ N. A. de Oliveira,⁶ A. A. Coelho,⁷ L. P. Cardoso,⁷ and J. A. Souza⁸

¹*Instituto de Física, Universidade Federal Fluminense - UFF, Av. Gal. Milton Tavares de Souza s/n, 24210-346, Niterói, RJ, Brazil*

²*Instituto de Ciências Tecnológicas e Exatas, Universidade Federal do Triângulo Mineiro (UFTM), 38066-200 Uberaba, Brazil*

³*Laboratório Nacional de Luz Síncrotron, CNPEM, 13083-970 Campinas, SP, Brazil*

⁴*Universidade Federal do Maranhão, CCSST, Imperatriz, MA, 65900-410, Brazil*

⁵*Departamento de Ciências Exatas e da Terra, Universidade Federal de São Paulo, Diadema, 09972-270, SP, Brazil*

⁶*Instituto de Física Armando Dias Tavares, Universidade do Estado do Rio de Janeiro - UERJ,*

Rua São Francisco Xavier, 524, 20550-013 RJ, Brazil

⁷*Instituto de Física Gleb Wataghin, Universidade Estadual de Campinas - UNICAMP,*

Caixa Postal 6165, 13083-859 Campinas, S. Paulo, Brazil

⁸*Universidade Federal do ABC-Santo André, São Paulo 09210-580, Brazil*

(Received 4 December 2015; revised manuscript received 10 February 2016; published 29 February 2016)

This paper presents the results of an investigation of the magnetic and structural properties of $\text{Mn}_{1-x}\text{Fe}_x\text{As}$ compounds under hydrostatic pressure and chemical doping. The chemical doping was performed by using low Fe doping levels ($x = 0, 0.003, 0.006, 0.010, 0.015, \text{ and } 0.018$), which emulates the negative pressure effect on the crystal structure. The results of this approach were compared with the physical pressure effect (hydrostatic pressure from 0 to 2.2 kbar) on the $\text{Mn}_{0.997}\text{Fe}_{0.003}\text{As}$. Both approaches exhibit the same magnetic behaviors: the T_C and saturation magnetization decrease as the pressure increases; for the highest pressure studied, an orthorhombic antiferromagnetic phase occurs below the critical temperature and coexists with the ferromagnetic hexagonal phase. The equivalence between hydrostatic pressure and chemical doping indicates that the Fe doping only causes structural deformation. In addition, we performed magnetic measurements at high temperature (up to 520 K) on the samples with $x = 0$ and 0.003 in order to investigate the magnetic behavior above $T_C = 310$ K. These results, along with structural characterization, clearly show that between T_C and T_I the system is a weak antiferromagnet with short-range order confined only in the ab plane. Finally, using the low- and high-temperature data, the magnetic phase diagrams of the compound under hydrostatic pressure and chemical doping were redrawn.

DOI: [10.1103/PhysRevB.93.054431](https://doi.org/10.1103/PhysRevB.93.054431)

I. INTRODUCTION

The MnAs compound and its derivatives have been extensively studied owing to their intense magnetocaloric effect (MCE) around room temperature [1,2], making them very promising materials for magnetic refrigeration. The high MCE values are associated with the magnetic transition, which is accompanied with a structural modification from the α -phase, hexagonal NiAs-type (magnetically ordered) structure, to β -phase, orthorhombic MnP-type (unordered) structure. The compound undergoes another structural transition from orthorhombic (β phase) to hexagonal (γ phase) at $T_I = 398$ K [3]. Above T_I , the material is paramagnetic and follows the Curie-Weiss law, while at temperatures between T_C and T_I it is frequently considered paramagnetic but does not follow the Curie-Weiss law [4]. Moreover, no long-range magnetic orders were detected in this compound in neutron scattering experiments [5,6].

The magnetic properties (such as, T_C and saturation magnetization) can be modified by changing the interatomic distance. This structural modification can be achieved by either applying hydrostatic pressure or chemical doping. The chemical doping can be performed by partially replacing Mn or As with other elements. Substitution of As with Sb

has been successfully performed by Wada *et al.* [7]. The authors prepared single-phase $\text{MnAs}_{1-x}\text{Sb}_x$ compounds and observed that the substitution of 10% Sb for As reduces the thermal hysteresis while the giant magnetocaloric properties are retained. Mn substitution was more explored than As, it is possible to find a variety of previous research where the Mn is replaced with other transition metals, as for example Fe [1], Cu [8], V [9], Cr, Ti [9], and Co [10,11]. The pressure effect (contraction or expansion of the unit cell) is achieved by the difference between the mean ionic radii of the elements; however, when Mn is replaced with other transition metals, it is necessary in some cases, to consider the valence electron concentration since the conduction electrons play a fundamental role in the itinerant magnetism.

Hydrostatic pressure (external pressure) has many advantages over its chemical counterpart (chemical doping) as for example the hydrostatic pressure retains the composition, purity, and shape of the sample. Thus the use of hydrostatic pressure provides a clean way of studying the pressure effect on magnetic properties. Earlier studies using hydrostatic pressure on the MnAs compound have showed a remarkable dependence of the Curie temperature on the pressure (up to 2.2 kbar) [2,12]. Studies conducted by Goodenough [13] and Menyuk [14] have also shown remarkable changes in the structural and magnetic properties on the application of higher pressures (up to 11 kbar). The main finding of these works was that the hexagonal phase is no longer stable at

*rocco@if.uff.br

pressures above 4.6 kbar and the orthorhombic phase (β phase) is observed over the entire temperature range. In addition, the results show that at pressures between 3 and 4.6 kbar, an orthorhombic structure with long-range antiferromagnetic (AFM) order occurs at temperatures below 230 K and seems to coexist with a ferromagnetic (FM) state down to ~ 50 K, when the FM phase transforms into AFM phase. This is very interesting as it supports the results of recent works [15] that claim that the orthorhombic phase above the critical temperature (β phase) consists of AFM planes of Mn but that the exchange coupling between the planes is so weak that their ordering is random. This randomness accounts for the failure of neutron scattering to detect long-range AFM order [5,6]. The antiferromagnetic order between T_C and T_I has already been suggested by Guillaud [16] but the absence of long-range order revealed by neutron diffraction was always considered an evidence against the AFM order.

In order to shed light on the magnetic and structural phases induced by chemical doping and hydrostatic pressure applied to $\text{Mn}_{1-x}\text{Fe}_x\text{As}$ compounds, we present a structural and magnetic study where a very low Fe doping level is used to emulate the pressure effect on MnAs. Section II shows the structural properties of these compounds, which were investigated by both conventional x-ray diffraction and synchrotron radiation. This latter was performed as a function of temperature from ~ 100 to 380 K for the compound with the highest doping level, $\text{Mn}_{0.9825}\text{Fe}_{0.018}\text{As}$, which reveal a phase coexistence below 210 K. The conventional x-ray diffraction was performed just below (270 K) and above the critical temperature (333 K) in order to monitor the unit cell volume of the α and β phases as a function of Fe doping level. These results reveal that the chemical doping stabilizes the orthorhombic structure. In Sec. III, the magnetic properties of $\text{Mn}_{1-x}\text{Fe}_x\text{As}$ compounds are detailed with emphasis on the magnetization at high temperature and the magnetic configuration of the β -phase between T_C and T_I is discussed. These magnetic data are compared to those of $\text{Mn}_{0.997}\text{Fe}_{0.003}\text{As}$ subjected to hydrostatic pressure, presented in Sec. IV. Finally, the results are discussed in Sec. V, which show complete agreement between the two approaches (chemical doping and physical pressure); moreover, the magnetic phase diagrams for $\text{Mn}_{1-x}\text{Fe}_x\text{As}$ under hydrostatic pressure and chemical doping could be redrawn.

II. EXPERIMENTAL AND STRUCTURAL PROPERTIES

The samples of $\text{Mn}_{1-x}\text{Fe}_x\text{As}$ (with $x = 0, 0.003, 0.006, 0.01, 0.015$ and 0.018) were prepared following the route presented in Ref. [1]. The magnetic measurements were performed in a SQUID magnetometer and for measurements under hydrostatic pressure we used a CuBe cell. The pressure was determined monitoring the critical temperature of a Pb piece placed together with the sample. High-energy x-ray diffraction experiments as a function of temperature were performed on $\text{Mn}_{0.9825}\text{Fe}_{0.018}\text{As}$ at the 11-ID-C beamline of the Advanced Photon Source (APS) at Argonne National Laboratory (ANL). Polycrystalline powder of the sample was placed into kapton capillaries, and rotated in a spinner during the diffraction experiments. Temperature-dependent measurements were carried out with an Oxford Cryostream Cooler 700

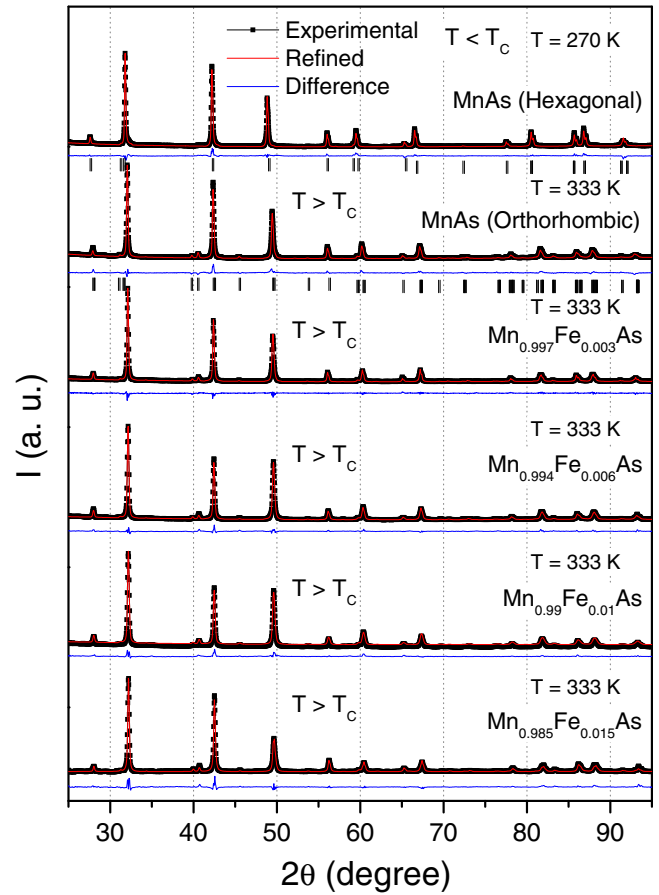


FIG. 1. X-ray diffraction patterns with the Rietveld refinement of the MnAs sample at $T = 270$ K $< T_C$ in the hexagonal phase (top) and in the orthorhombic phase (at $T = 333$ K $> T_C$) for almost all samples. Note that some peaks, around 40° , for instance, are observed in the orthorhombic phase but it disappears in the hexagonal phase. A displacement of the peaks to higher angles is observed as the Fe amount increases and when the system suffers the transition from the hexagonal to orthorhombic phase. These indicate that the lattice parameters decrease as x increases.

system. The temperature stability during the measurements was 0.1 K or better. Powder diffraction data were collected with a MAR345 image plate, calibrated with a CeO_2 standard, converted to 1D patterns with FIT2D [17], and analyzed with the Rietveld refinement program GSAS. The other samples were investigated using the conventional x-ray diffraction (XRD) with an X'Pert PRO MRD Philips diffractometer with radiation $\text{Cu K}\alpha$ (1.5405 \AA). The measurements were performed just below ($T = 270$ K) and above ($T = 333$ K) the critical temperature using a special set up with a Peltier cell coupled to a temperature controller. The diffractograms were analyzed by the Rietveld method (Fig. 1), which shows that the samples are single phase and crystallize in the hexagonal (spatial group $P6_3/mmc$) α phase below T_C (Fig. 1, top) with atomic positions of $(0,0,0)$ and $(1/3,2/3,1/4)$ for the Mn/Fe (Wyckoff number 2a and site $-3m$) and As (Wyckoff number 2c and site $-6m2$), respectively, and orthorhombic (spatial group $Pnma$) β -phase structure (Fig. 1) above T_C with atomic positions of $(0.997, 1/4, 0.233)$ and $(0.275, 1/4,$

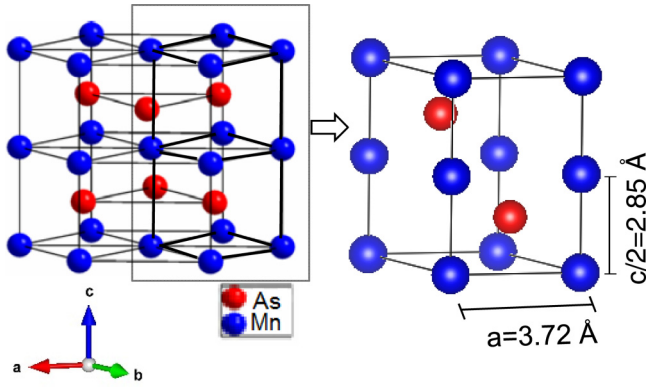


FIG. 2. (Left) Hexagonal structure of MnAs at temperatures below T_c . (Right) Single unit cell of the hexagonal structure showing the Mn-Mn distance in the a and c directions. Note that the first-nearest neighbors are along the c axis.

0.922) for the Mn/Fe (Wyckoff number 4c and site.m.) and As (Wyckoff number 4c and site.m.), respectively. Figure 2 (left) shows the hexagonal structure for MnAs, which is composed of alternating hexagonal planes of Mn and As atoms (ab planes). For $x = 0$, the Mn atom within the hexagonal plane has six second-nearest neighbors at a distance of 3.7229 \AA (length of the lattice parameters a and b), while the first nearest neighbors are along the c axis at a distance of $c/2 = 2.854 \text{ \AA}$, as indicated in Fig. 2 (right). As the amount of Fe increases, the unit cell volume of the hexagonal structure decreases (Fig. 3) with a rate of $-46 \text{ \AA}^3/\text{Fe atom}$ [or $(1/V)dV_{\text{hex}}/dx = 0.34 \text{ Fe}^{-1}$ for the normalized volume case], which is the effect of the smaller average ionic radius of Fe; thus, the Fe doping emulates the negative pressure effect. From Fig. 3, it is also seen that the c parameter of the hexagonal phase decreases more quickly than the a parameter; $da/dx = -0.13 \text{ \AA}/\text{Fe atom}$ [$(1/a)da/dx = 0.03 \text{ Fe}^{-1}$] and $dc/dx = -0.9 \text{ \AA}/\text{Fe atom}$ [$(1/c)dc/dx = 0.26 \text{ Fe}^{-1}$]. This indicates that the hexagonal planes become closer to each other as Fe replaces Mn, while

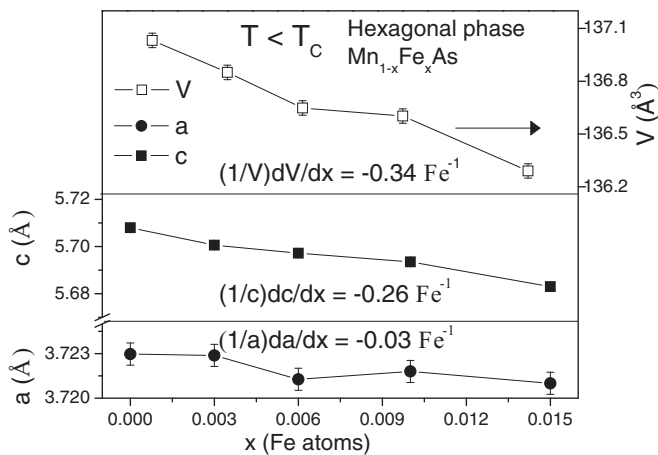


FIG. 3. Lattice parameters $a = b$, c and unit cell volume as a function of Fe content for all samples in the hexagonal phase. Lattice parameter c changes more quickly than a . The structural data for sample with $x = 0.018$ will be presented later.

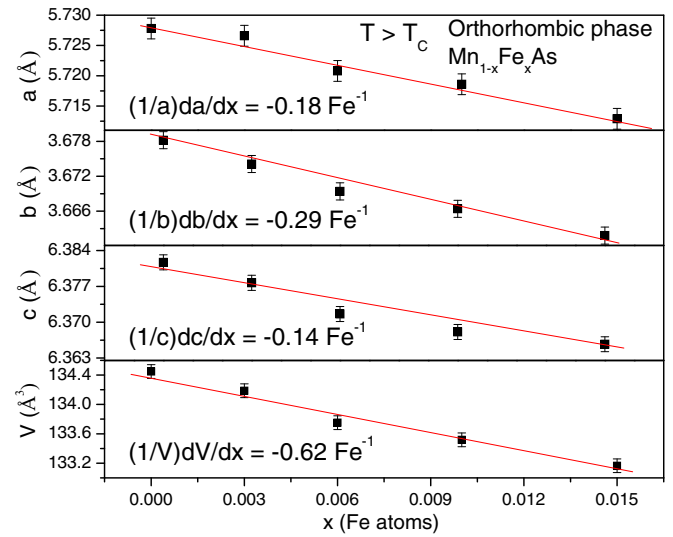


FIG. 4. Structural parameters of the orthorhombic structure as a function of Fe content for all samples at temperatures above T_c . The lattice parameters a , b , and c exhibit the same dependence on Fe content.

the basal plane (ab plane) seems to be relatively unaffected by the chemical doping. The x-ray diffraction above the critical temperature with the Rietveld analyzes are shown in Fig. 1, which shows that the orthorhombic structure (β phase) also exhibits a volume contraction as Mn atoms are replaced by the Fe atoms (Fig. 4). However, the decreasing rate for this structure is almost double [$dV_{\text{orth}}/dx = -86 \text{ \AA}^3/\text{Fe}$ or $(1/V)dV_{\text{orth}}/dx = -0.62 \text{ Fe}^{-1}$], because the structure suffers an isotropic contraction as revealed from the analysis of decreasing rate of lattice parameters ($da/dx \sim db/dx \sim dc/dx \sim -1 \text{ \AA}/\text{Fe}$ or $\sim -0.2 \text{ Fe}^{-1}$] for the normalized value case) in Fig. 4. It is evident that the lack of long-range order causes this homogeneous contraction.

By comparing the unit cell volumes of the hexagonal and orthorhombic structures, we observe that during the transition from the low-temperature phase (phase-ordered) to the high-temperature phase (phase-disordered) the volume is reduced by 1.88 % for $x = 0$ (Table I), and $\Delta V/V_0$ increases as Fe content increases. The reduction of volume is schematically

TABLE I. Unit cell volume of the hexagonal and orthorhombic structures and $\Delta V/V_0$.

$\text{Mn}_{1-x}\text{Fe}_x\text{As}$	$V_{\text{Hex.}}^a (\text{\AA}^3)$	$V_{\text{Orth.}} (\text{\AA}^3)$	$\Delta V/V_0 (\%)$
0	137.0(3)	134.4(4)	1.88
0.003	136.8(5)	134.1(6)	1.94
0.006	136.6(4)	133.7(5)	2.11
0.010	136.6(3)	133.5(2)	2.25
0.015	136.2(4)	133.1(3)	2.29

^aThe unit cell of the orthorhombic structure can be obtained from the hexagonal one by increasing twice the volume of the phase hexagonal, because the orthorhombic space group is a subgroup of the hexagonal one. Thus, for comparison purposes, the volume of the hexagonal structure was multiplied by two in table.

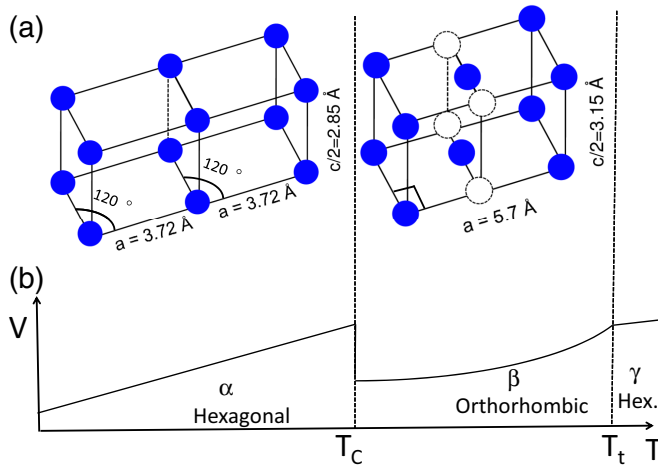


FIG. 5. (a) Schematic unit cell of the hexagonal structure (left) without considering the As atoms and orthorhombic structure (right) with the main distance between the Mn atoms (adapted from the Ref. [18]). The white circles represent the Mn site in the hexagonal structure. Note that the Mn-Mn distance along the c axis for the orthorhombic phase is higher than hexagonal one, and, still, that the first nearest neighbors of the Mn atoms are along the c axis in the hexagonal phase and are in the ab plane for the orthorhombic phase. (b) Structural phase diagram of MnAs (schematic plot adapted from the Ref. [19]). The unit cell of the orthorhombic structure can be obtained from the hexagonal one by increasing twice the volume of the phase hexagonal, because the orthorhombic space group is a subgroup of the hexagonal one. Thus, for comparison purposes, the volume of the hexagonal structure shown here is duplicated.

shown in Fig. 5(b), which also shows that the effect of transition on the structure is basically a contraction of the basal plane (ab plane) and the increase of the c lattice parameter, i.e., the distances between Mn atoms within the planes decrease as ab planes become farther apart. Thus, for the orthorhombic structure, the first nearest neighbors are in the ab plane, instead of along the c axis, at a distance of 2.894 Å (for $x = 0$), as shown in Fig. 5(a). The distance Mn-Mn in the c direction is 3.15 Å for the orthorhombic structure. This is an important point in the discussion on magnetic interactions.

Figure 6 shows the XRD using synchrotron radiation with the correspondent Rietveld refinement of the $\text{Mn}_{0.982}\text{Fe}_{0.018}\text{As}$ sample at $T = 180$ K. The peaks of the orthorhombic and hexagonal structures coexist at this temperature. In addition, this technique was performed in the temperature range from 120 to 398 K that showed that the sample with $x = 0.018$ exhibits a coexistence of $\sim 57\%$ of the hexagonal and $\sim 43\%$ of the orthorhombic phase between 120 and ~ 270 K, and above ~ 270 K the structure is pure orthorhombic because the hexagonal structure changes to the orthorhombic, as shown in Fig. 7(a). Goodenough *et al.* [13] have observed this phase coexistence by electrical resistance measurements with hydrostatic pressure. The authors found that above a critical pressure of 4.6 kbar a pure orthorhombic phase is stable in the whole temperature range; however, between 2 and 4.6 kbar, a metastable region is always observed below the critical temperature. These results indicate that the hydrostatic pressure stabilizes the orthorhombic structure.

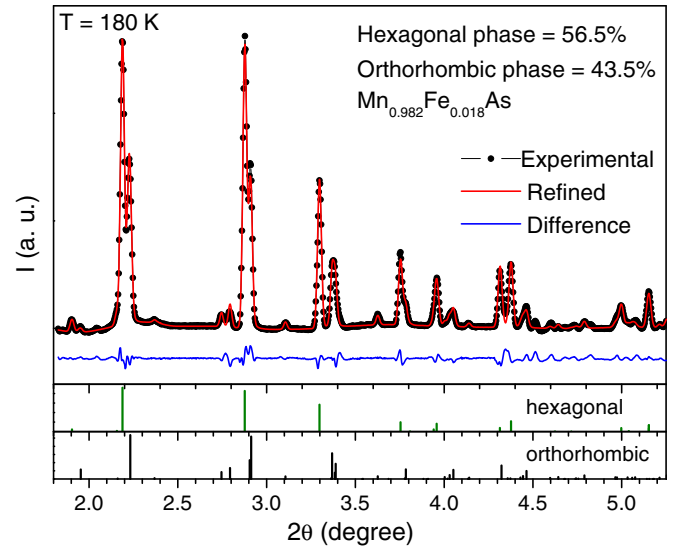


FIG. 6. X-ray diffraction using synchrotron radiation with the correspondent Rietveld refinement of the $\text{Mn}_{0.982}\text{Fe}_{0.018}\text{As}$ sample at $T = 180$ K. Note that the peaks of the orthorhombic and hexagonal phases coexist at this temperature.

Figure 7(b) shows the unit cell volume of both structures as a function of temperature; the volume of the orthorhombic structure increases almost linearly from 125 to 200 K, and at 210 K, the lattice parameters a , b , and c drastically increase producing an abrupt volume change. Interestingly, the volume of the orthorhombic phase always increases with increasing temperature. It should be noted that the temperature at which the volume of the orthorhombic phase changes and the temperature of hexagonal transformation are considerably different. This observation is very important for the discussion of the sample magnetic properties.

III. MAGNETIZATION UNDER CHEMICAL DOPING

The decrease of unit cell volume observed in Figs. 3 and 4 should influence the magnetic properties greatly, since the magnetic interaction is very sensitive to the interatomic distance. Figures 8(a) and 8(b) show these results, where it is possible to see an abrupt magnetic transition at T_C [Fig. 8(a)] for three samples (the curves for the other samples can be seen in Ref. [1]), which also defines structural transition from the hexagonal phase (below T_C) to orthorhombic (above T_C) phase. The transition displaces to lower temperatures and the thermal hysteresis markedly increases as the unit cell volume decreases (Fe content increases). This result clearly shows that the contraction of the unit cell volume makes the hexagonal structure less stable. This agrees very well with Menyuk's [14] work, which shows that above 4.2 kbar, the volumetric contraction is too high making the hexagonal phase unstable; consequently, the orthorhombic phase is stabilized over the entire temperature range. In this case, a long-range AFM state occurs at low temperature (below the critical temperature) instead of the FM state. Wada *et al.* have also argued that the hexagonal structure disappears and the AFM state appears at the critical pressure slightly lower (2.5 kbar). This information, along with the x-ray data presented in Fig. 7, explain the result

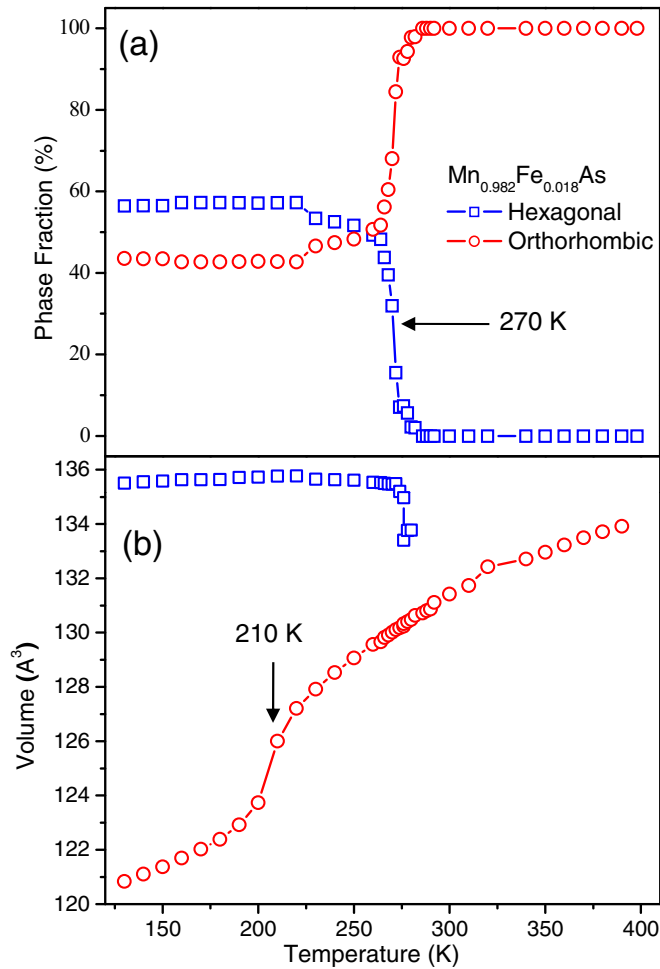


FIG. 7. (a) Phase fraction of the hexagonal and orthorhombic structures as a function of temperature and at ambient pressure for the sample $\text{Mn}_{0.982}\text{Fe}_{0.018}\text{As}$. (b) Unit cell volume of the hexagonal and orthorhombic structures as a function of temperature. The measurements were performed increasing the temperature.

in Fig. 8(b) that shows the $M(T)$ curve of the $\text{Mn}_{0.982}\text{Fe}_{0.018}\text{As}$ sample, which exhibits the smallest unit cell volume and phase coexistence. In that curve, two transitions exist; one at $T_N = 210$ K is from the orthorhombic-AFM (AFM with long-range order) phase (below 210 K) to orthorhombic β phase (above 210 K), and the other at $T_C = 275$ K is from the hexagonal-FM to the same orthorhombic β phase. Note the AFM transition occurs between the two orthorhombic phases with a huge volume variation of $(\Delta V/V_0 \sim 2\%)$, and that the volume before this transition is smaller than that after the transition, as opposed to the transition from hexagonal to orthorhombic.

As seen before, the Fe doping (for larger x) stabilizes the orthorhombic phase that coexists with the hexagonal below the critical temperature, and the orthorhombic phase is AFM below T_N . Thus the samples with coexisting phases are expected to exhibit lower saturation magnetization (M_S) than those with a FM ground state ($x \leq 0.010$). The magnetization curves as a function of applied magnetic field at 4 K are presented in Fig. 9; as expected the sample with coexisting phases at low temperature exhibits a saturation magnetization

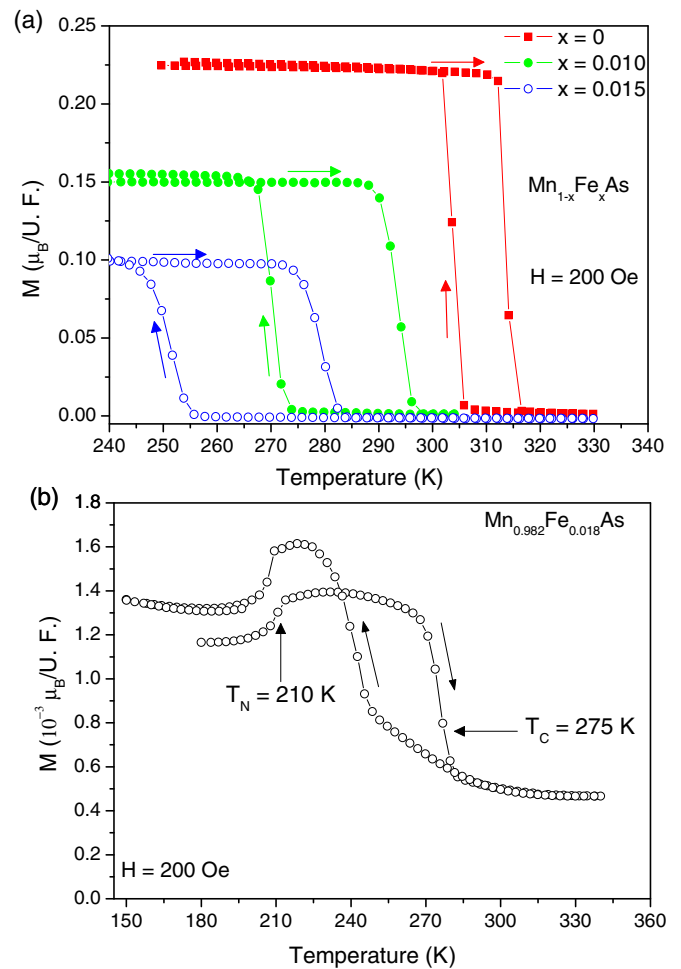


FIG. 8. (a) Magnetization as a function of temperature with 200 Oe of applied magnetic field for some $\text{Mn}_{1-x}\text{Fe}_x\text{As}$ compounds. The curves for the other compounds can be found in Ref. [1]. (b) Curve for samples with $x = 0.018$ showing the two transitions from the hexagonal-ferromagnetic and the orthorhombic-antiferromagnetic to orthorhombic-paramagnetic phase. The lines are guides to the eye.

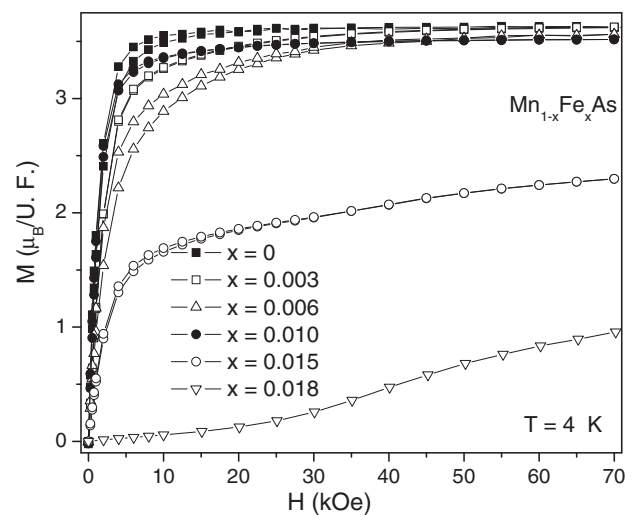


FIG. 9. Magnetization as a function of applied magnetic field at 4 K for $\text{Mn}_{1-x}\text{Fe}_x\text{As}$ compounds.

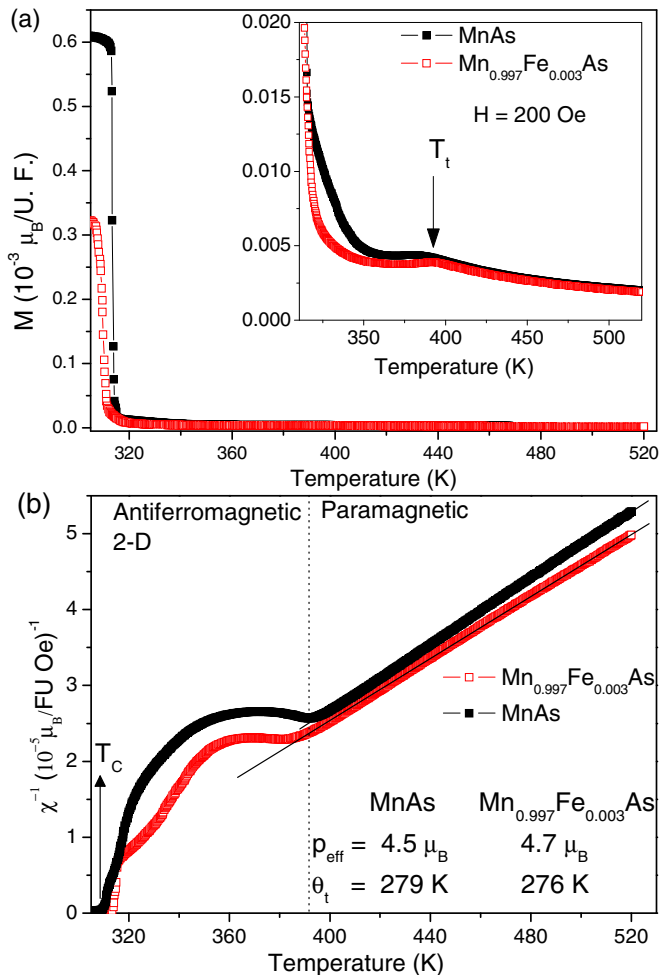


FIG. 10. (a) Magnetization curves of MnAs and $\text{Mn}_{0.997}\text{Fe}_{0.003}\text{As}$ compounds as a function of high temperature (until 520 K) with 200 Oe of applied magnetic field. In the inset, it is possible to see that between T_C and T_t the magnetization follows a different tendency than above T_t . Panel (b) clarifies this behavior. (b) Inverse susceptibility as a function of temperature for the $\text{Mn}_{0.997}\text{Fe}_{0.003}\text{As}$ and MnAs compounds showing two magnetic regions; antiferromagnetic 2D and paramagnetic. By adjusting the paramagnetic region using the Curie-Weiss law, it was possible to obtain the effective moment and paramagnetic Curie temperature.

smaller than the one with a FM ground state. For samples with $x \leq 0.01$, the M_S is approximately $3.5 \mu_B$, which agrees very well with previous results for the MnAs compound [20]. However, for samples with $x > 0.01$, a significant decrease in M_S is observed. For $x = 0.015$, no phase coexistence (data not shown here) is observed below the critical temperature down to 100 K. But, a hexagonal AFM phase below 50 K was already observed [14] for MnAs under low hydrostatic pressure. Therefore we are convinced that the lower magnetization for this sample at 4 K is due to this effect.

Some researchers claim that the orthorhombic structure between T_C and T_t for the FM samples [Fig. 8(a)] is not paramagnetic, but is, instead, weakly AFM. This is reasonable since the orthorhombic structure is associated with the AFM behavior, as shown in Fig. 8(b). To verify if our samples exhibit this behavior, we performed magnetic measurements

at high temperature (above T_C) for two samples: $x = 0$ and 0.003. Figure 10(a) shows the $M \times T$ curves; the inset shows that above the transition (310 K) the curves exhibit unusual behavior. This is better demonstrated in Fig. 10(b), which shows the inverse susceptibility versus temperature. From these curves, it is evident that both samples follow the Curie-Weiss law above 390 K, with an effective moment (p_{eff}) of 4.5 and $4.7 \mu_B$ and a paramagnetic Curie temperature θ_t of 279 and 276 K, respectively. These values are in very good agreement with Menyuk and Goodenough's reports [13,14]. However, for temperatures between T_C and T_t , the material is very far from a genuine paramagnetic behavior. Theoretical studies using density functional [15] and first-principles calculations [19] have demonstrated that the orthorhombic distortion in the β phase induces the AFM order. Both studies show that in the β phase the AFM state occurs in the planes of Mn (ab planes) and the exchange coupling between the planes is so weak that the ordering of planes is random, resulting in the formation of a two-dimensional AFM state with short-range order. Therefore we will refer to the state between T_C and T_t as two-dimensional short-range AFM (2D-SR-AFM). This conclusion is supported by our structural data, which show that the first nearest neighbors of Mn are along the c axis in the hexagonal phase, but when the material suffers the transition to the orthorhombic phase, the first nearest neighbors of the Mn atoms lie in the ab planes. Thus it is supposed that during the transition from the α to β phase the magnetism between the planes is disconnected, but the Mn atoms of the basal plane remain magnetically connected by means of the AFM state with short-range order.

IV. HYDROSTATIC PRESSURE

As discussed before, the hydrostatic pressure provides a clean way of studying the pressure effect on the magnetic properties, because it retains the composition, the purity, and shape of the sample, thus, we performed magnetic measurements on the $\text{Mn}_{0.997}\text{Fe}_{0.003}\text{As}$ compound under hydrostatic pressure. Our main goal is to verify whether our findings presented before are only an effect of the volume change or they are due to the iron atoms providing a change in the electronic structure of the material. The magnetization as a function of temperature for different pressures is presented in Figs. 11(a) and 11(b), and it shows a displacement of T_C for lower temperatures with a rate of -16.8 K/kbar (for increasing temperature and -25.1 K/kbar for decreasing temperature), and a large thermal hysteresis is also found, whose value increases with the pressure from 18 to 33 K for 0 and 1.9 kbar, respectively, which corresponds to a rate of 8.3 K/kbar . These values are in agreement with other results [13]. The dependence on T_C and the hysteresis with the physical pressure are exactly the same as with chemical doping, and another similarity between the two approaches is the shape of the M versus T curve at higher pressures (2.2 kbar) shown in Fig. 11(b). That curve shows that the pressure (chemical doping) stabilizes a regime of phase coexistence, because, as before, it exhibits two transitions; one of them is at 219 K from the orthorhombic-AFM with long-range order (below T_N) to the pure orthorhombic phase (above T_N), and the other one is from the hexagonal-FM to the pure orthorhombic at 269 K. The magnetization as a function of the applied magnetic field for the sample under hydrostatic

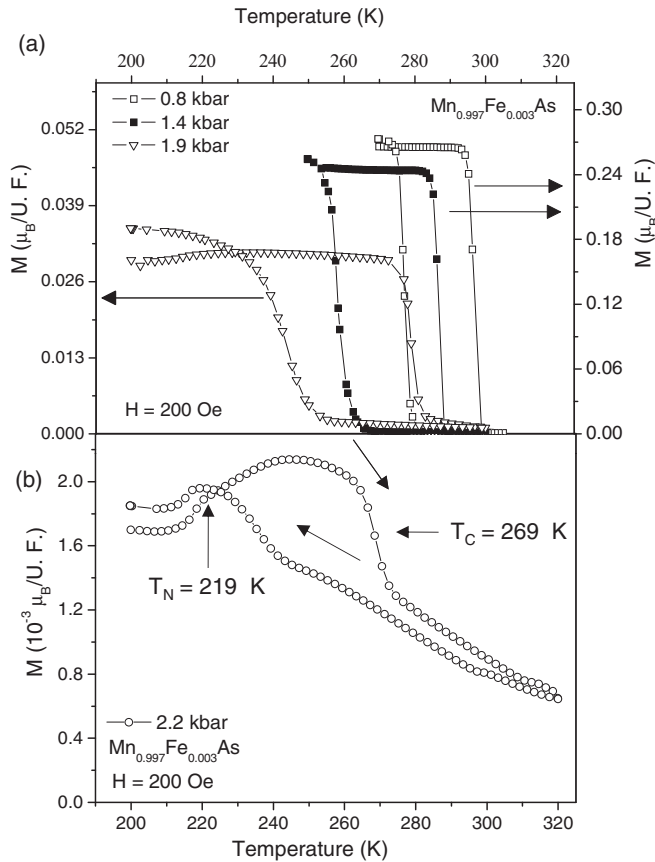


FIG. 11. (a) Magnetization as a function of temperature with 200 Oe of applied magnetic field for the $Mn_{0.997}Fe_{0.003}As$ compound under hydrostatic pressures of 0.8, 1.4, and 1.9 kbar. (b) The M vs T curve for the sample under the highest applied pressure (2.2 kbar) indicating the temperature of the antiferromagnetic and ferromagnetic transitions.

pressure is presented in Fig. 12. For ambient pressure, the saturation magnetization (M_S) is around $3.5 \mu_B$ and as the pressure increases, M_S decreases (Fig. 12), as before, due to

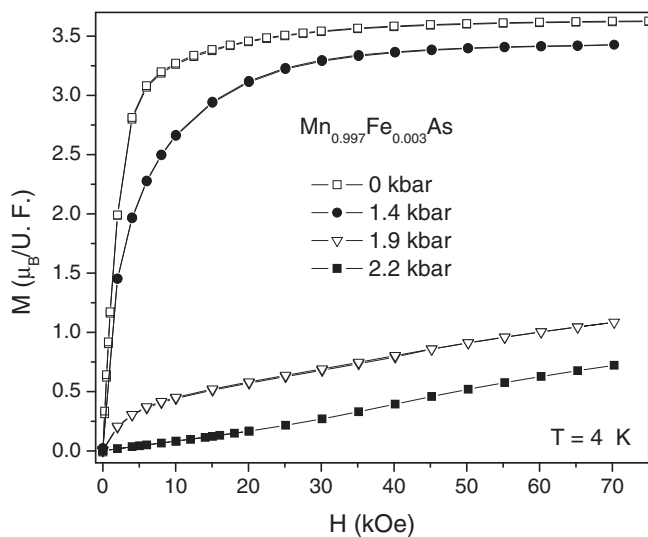


FIG. 12. Magnetization as a function of applied magnetic field for all hydrostatic pressures applied on $Mn_{0.997}Fe_{0.003}As$ at 4 K,

the AFM state stabilization at low temperature. These magnetic data show that a regime of phase coexistence is stabilized at pressures larger than 1.9 kbar for the $Mn_{0.997}Fe_{0.003}As$ sample. This limit is slightly smaller than that one for MnAs presented by the Menyuk [14] and Goodenough's works [13]. All these magnetic data show that the orthorhombic phase between T_C and T_i is the same as defined before, which consists of AFM planes with short-range interaction and with very weak exchange coupling between planes (2D-SR-AFM state).

V. OVERVIEW OF THE RESULTS AND MAGNETIC PHASE DIAGRAM

It is well known that the orthorhombic structure is stabilized when the unit cell volume is reduced, and, as seen before, this can be reached either during the magnetic transition around the critical temperature or by using hydrostatic pressure or chemical doping. When one is using the pressure approach,

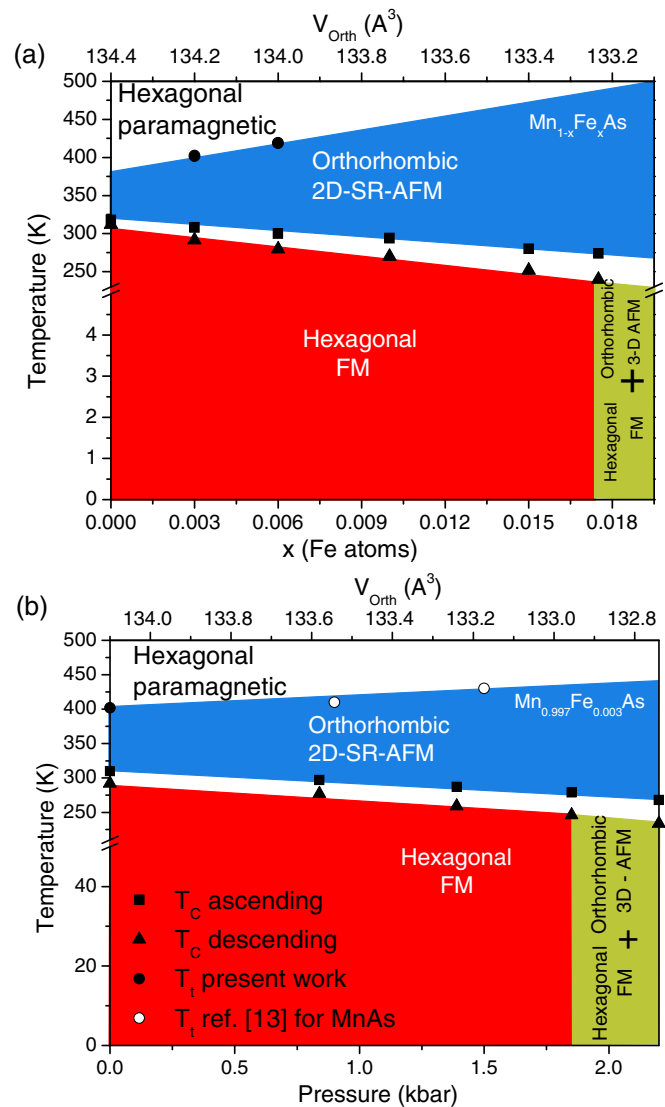


FIG. 13. Magnetic phase diagrams for the $Mn_{1-x}Fe_xAs$ system (a) and for the $Mn_{0.997}Fe_{0.003}As$ compound under hydrostatic pressure (b). The open circles (\circ) are data taken from Ref. [13] for the MnAs compound.

the orthorhombic phase appears below the magnetic transition coexisting with the hexagonal phase for a hydrostatic pressure between 2.2 kbar and 4.6 kbar according to Goodenough and Menyuk [13,14] and above 1.9 kbar according to the present work. Above 4.6 kbar, the hexagonal phase disappears [13,14] and only the orthorhombic one survives. It is also well established that the orthorhombic phase that coexists with the hexagonal is AFM [14], and our magnetic measurements presented in Figs. 8(b) and 11(b) show such evidence for the samples at the highest pressures and chemical doping level. The low-temperature hexagonal phase is FM with the first nearest neighbors of the Mn atoms along the c axis, but when the material suffers the transition to the orthorhombic phase, a remarkable change in the Mn-Mn distance occurs in such a way that the first nearest neighbors of Mn are in the ab planes. This produces a change in the exchange interaction such that the magnetism between planes is turned off, but the Mn atoms of the basal plane remain magnetically connected by means of a short-range AFM interaction. Thus we redrew the magnetic phase diagram of the $\text{Mn}_{0.997}\text{Fe}_{0.003}\text{As}$ under hydrostatic, Fig. 13(b), and chemical doping, Fig. 13(a), taking into account that the orthorhombic phase between T_C and T_I is a 2D-SR-AFM instead of paramagnetic. In addition, we redefine the critical pressure in which the $\text{Mn}_{0.997}\text{Fe}_{0.003}\text{As}$ system exhibits a phase coexistence.

Finally, using the compressibility values of MnAs [1,14] ($4.55 \times 10^{-11} \text{ Pa}^{-1}$), we calculated the correspondent unit cell volume for each hydrostatic pressure. The values are shown in Figs. 13(a) and 13(b), and we can see a very good agreement between the volume change of the compounds under hydrostatic pressure and chemical doping.

VI. CONCLUSION

In this work, we produced samples of the magnetocaloric compound $\text{Mn}_{1-x}\text{Fe}_x\text{As}$ with a low Fe doping level ($x = 0, 0.003, 0.006, 0.01, 0.015, \text{ and } 0.018$) in order to emulate a negative pressure effect on the crystal structure. These samples were characterized by conventional x-ray diffraction just below and above the magnetic transition temperature, which showed that the unit cell volume (hexagonal and orthorhombic)

decreases as the Fe content increases, which ratifies the negative pressure effect of Fe. In addition, we compared the distance between the Mn atoms in the two structures and we found that in the hexagonal phase, for $x = 0$, for example, the first nearest neighbors of Mn are along the c axis at a distance of $c/2 = 2.854 \text{ \AA}$, and that in the orthorhombic phase the first nearest neighbors are in ab planes at a distance of 2.894 \AA . This is a remarkable finding since the hexagonal phase is FM, while the orthorhombic phase exhibits no long-range magnetic order. Thus we are convinced that during the transition from α to β phase the magnetism between planes is turned off, but the Mn atoms of the basal plane remain magnetically connected by means of a short-range antiferromagnetic interaction. This is ratified by the theoretical works [15,19] and by magnetic measurements performed at high temperatures (between T_C and T_I), which shows that in this temperature range the samples do not follow the Curie-Weiss law. The x-ray diffraction using synchrotron radiation as a function of temperature performed in the sample $\text{Mn}_{0.982}\text{Fe}_{0.018}\text{As}$ showed a phase coexistence of the orthorhombic and hexagonal phases below the critical temperature, which indicates that the pressure stabilizes the orthorhombic phase. The magnetization data for these samples show that the orthorhombic phase, which appears below T_C , is an AFM with long-range order, fortifying, thus, the idea of a 2D AFM state in the orthorhombic phase above the magnetic transition. Yet, the magnetic measurements for the samples with different Fe doping levels show that the critical temperature decreases as Fe increases, and that the saturation magnetization for the sample with the highest x value is reduced due to the AFM phase. These magnetic data for chemical doping were compared with the data of $\text{Mn}_{0.997}\text{Fe}_{0.003}\text{As}$ under hydrostatic pressure of up to 2.2 kbar, and the complete equivalence between the two approaches was verified. With these findings it was possible to redraw the magnetic phase diagram as a function of hydrostatic and chemical doping, where the critical pressure for the appearance of the phase coexistence regime is redefined.

ACKNOWLEDGMENTS

The authors would like to thank to CNPq, CAPES, FAPERJ, FAPEMIG, FAPESP, and PROPPI-UFF for financial support.

-
- [1] A. Campos, D. L. Rocco, A. M. G. Carvalho, L. Caron, A. A. Coelho, S. Gama, L. M. Silva, F. C. G. Gandra, A. O. Santos, L. P. Cardoso, P. J. von Ranke, and N. A. Oliveira, *Nat. Mater.* **5**, 802 (2006).
 - [2] S. Gama, A. A. Coelho, A. de Campos, A. M. G. Carvalho, F. C. G. Gandra, P. J. von Ranke, and N. A. de Oliveira, *Phys. Rev. Lett.* **93**, 237202 (2004).
 - [3] H. Wada, S. Matsuo, and A. Mitsuda, *Phys. Rev. B* **79**, 092407 (2009).
 - [4] J. N. Gonçalves, V. S. Amaral, J. G. Correia, and A. M. L. Lopes, *Phys. Rev. B* **83**, 104421 (2011).
 - [5] G. E. Bacon and R. Street, *Nature (London)* **175**, 518 (1955).
 - [6] R. H. Wilson and J. S. Kasper, *Acta Crystallogr.* **17**, 95 (1964).
 - [7] H. Wada and Y. Tanabe, *Appl. Phys. Lett.* **79**, 3302 (2001).
 - [8] D. L. Rocco, A. de Campos, A. M. G. Carvalho, L. Caron, A. A. Coelho, S. Gama, F. C. G. Gandra, A. O. dos Santos, L. P. Cardoso, P. J. von Ranke, and N. A. de Oliveira, *Appl. Phys. Lett.* **90**, 242507 (2007).
 - [9] M. Balli, D. Fruchart, D. Gignoux, C. Dupuis, A. Kedous-Lebouc, and R. Zach, *J. Appl. Phys.* **103**, 103908 (2008).
 - [10] K. Selte, A. Kjekshus, A. F. Andresen, and A. Zieba, *J. Phys. Chem. Solids* **38**, 719 (1977).
 - [11] A. Ziba, R. Zach, H. Fjellvåg, and A. Kjekshus, *J. Phys. Chem. Solids* **48**, 79 (1987).
 - [12] R. W. De Blois and D. S. Rodbell, *Phys. Rev.* **130**, 1347 (1963).
 - [13] J. B. Goodenough and J. A. Kafalas, *Phys. Rev.* **157**, 389 (1967).

- [14] N. Menyuk, J. A. Kafalas, K. Dwight, and J. B. Goodenough, *Phys. Rev.* **177**, 942 (1969).
- [15] M. K. Niranjan, B. R. Sahu, and L. Kleinman, *Phys. Rev. B* **70**, 180406 (2004).
- [16] C. Guillaud, *J. Phys. Radium* **12**, 223 (1951).
- [17] B. H. Toby, *J. Appl. Crystallogr.* **34**, 210 (2001).
- [18] I. Rungger and S. Sanvito, *Phys. Rev. B* **74**, 024429 (2006).
- [19] J. Łażewski, P. Piekarczyk, and K. Parlinski, *Phys. Rev. B* **83**, 054108 (2011).
- [20] L. H. Schwartz, E. L. Hall, and G. P. Felcher, *J. Appl. Phys.* **42**, 1621 (1971).